# Correspondence

## Generalized Probabilistic Scale Space for Image Restoration

Alexander Wong, *Member, IEEE*, and Akshaya K. Mishra, *Member, IEEE*

***Abstract*—A novel generalized sampling-based probabilistic scale space theory is proposed for image restoration. We explore extending the definition of scale space to better account for both noise and observation models, which is important for producing accurately restored images. A new class of scale-space realizations based on sampling and probability theory is introduced to realize this extended definition in the context of image restoration. Experimental results using 2-D images show that generalized sampling-based probabilistic scale-space theory can be used to produce more accurate restored images when compared with state-of-the-art scale-space formulations, particularly under situations characterized by low signal-to-noise ratios and image degradation.**

***Index Terms*—Bayesian, estimation, generalized, image restoration, noise, nonlinear, probabilistic, sampling, scale space.**

### I. Introduction

A powerful approach to multiscale decomposition and analysis that has gained significant popularity in the research community is scale-space theory [1], which is a framework for handling the inherent multiscale nature of the physical world by representing them across multiple scales, with a monotonic decrease in fine-scale structures being represented at each successive scale. One of the motivations for scale-space theory stems from the idea that, given no prior information about the scale of structures, the only reasonable course of action is to represent them at multiple scales [2]. Scale-space theory has become a particularly powerful tool in pattern recognition and image processing and has been widely used in feature detection [2]–[5], noise reduction [5]–[8], segmentation [9]–[13], classification [14], and color constancy enhancement [15].

While scale-space theory has been shown to be a very powerful, robust tool for computer vision applications [16], the application of scale-space theory in the context of image restoration has been largely limited to noise reduction [5]–[8]. Given that images are often subject to not only noise but also observation-based degradations, which has been largely unexplored in the context of scale-space theory, investigating the extension of scale-space theory to account for both noise and observation models can yield potential benefits for producing accurately restored images.

In this study, we propose a novel generalized sampling-based scale-space framework based on probability theory for the purpose of image restoration. The underlying goal of this generalized sampling-based probabilistic scale-space theory is to extend the definition of scale space to better account for noise and observation models, which are important for producing accurately restored images. We study nonlinear scale-space theory based on the generalized diffusion equation proposed by Perona and Malik [3] from a sampling and probabilistic point of view and derive a sampling-based probabilistic scale-space formulation that better satisfies the extended scale-space definition for image restoration under an identity observation model. We then derive a generalized sampling-based probabilistic scale-space formulation that satisfies the extended scale-space definition for image restoration under nonidentity observation models.

This paper is organized as follows. Previous scale-space formulations are reviewed in Section II. Scale-space realizations derived using the generalized diffusion equation is studied based on sampling and probability theory, and the sampling-based probabilistic scale-space formulation is derived in Section III. The generalized sampling-based probabilistic scale-space formulation is derived in Section IV. Finally, experimental results involving the restoration of 2-D images using the proposed sampling-based probabilistic scale-space formulation under different noise and degradation scenarios are presented in Section V, and conclusions are drawn in Section VI.

### II. Existing Scale-Space Formulations

Let $S$ be a set of sites into a discrete lattice $\mathcal{L}$ and $s \in S$ be a site in $\mathcal{L}$. Let $X = \{X_s | s \in S\}$, $Z = \{Z_s | s \in S\}$, and $N = \{N_s | s \in S\}$ be random fields on $S$, where $X_s$, $Z_s$, and $N_s$ take on values representing the state, observation, and observation noise at site $s$, respectively. Let $x = \{x_s | s \in S\}$, $z = \{z_s | s \in S\}$, and $n = \{n_s | s \in S\}$ be realizations of $X$, $Z$, and $N$, respectively, such that, given an observation model $H$, we have

$$z_s = Hx_s + n_s. \tag{1}$$

Scale-space theory attempts to represent $x_s$ as a single-parameter family of derived realizations $l_{s,t}$, where $t$ is a scaling parameter that defines the scale of structures in $x_s$ being represented. As first formalized by Witkin [1] and Koenderink and Van Doorn [17], an $m$-dimensional scale-space realization $l_{s,t}$ can be defined as the convolution of $l_{s,0} = z_s$ with a Gaussian function $G$ of variance $t$ as

$$l_{s,t} = \int_a G_{a,t} z_{s-a} da \tag{2}$$

$$G_{a,t} = \prod_{i=1}^{m} \frac{1}{\sqrt{2\pi t}} \exp\left[-\frac{a_i^2}{2t}\right]. \tag{3}$$

This linear scale realization can be equivalently defined as the solution to the diffusion equation [17]

$$\partial l_t = \frac{1}{2}\nabla^2 l \tag{4}$$

where $\nabla^2$ is the Laplacian. The linear scale-space formulation has been successfully used in a wide variety of computer vision applications [16], and scale-selection methods have been proposed for the linear scale-space formulation for robust feature detection [2].

Subsequent work by Perona and Malik [3] proposed that nonlinear scale-space realizations can be defined by extending to the solution of the generalized diffusion equation

$$\partial l_t = c_{s,t}\nabla^2 l + \nabla c_{s,t} \cdot \nabla l \tag{5}$$

Manuscript received April 18, 2009; revised March 09, 2010. First published April 22, 2010; current version published September 17, 2010. The associate editor coordinating the review of this manuscript and approving it for publication was Dr. Eero P. Simoncelli.

The authors are with the University of Waterloo, Waterloo, ON, Canada N2L 3G1 (e-mail: a28wong@uwaterloo.ca; akmishra@uwaterloo.ca).

Digital Object Identifier 10.1109/TIP.2010.2048973

where $c_{s,t}$ is the conduction coefficient, and $\nabla$ is the gradient. As such, the linear scale space becomes a special case of this nonlinear scale space where $c_{s,t} = 1/2$. Furthermore, Perona and Malik reasons that immediate localization and piecewise smoothing are important criteria to consider [3] and proposed the use of a nonnegative conduction coefficient that is a function of the gradient magnitude to better satisfy these criteria

$$c_{s,t} = \exp\left[-\left(\frac{\|\nabla l_{s,t}\|}{\kappa}\right)^2\right]. \tag{6}$$

This conduction coefficient discourages diffusion when $\|\nabla l_{s,t}\|$ is large and encourages diffusion when $\|\nabla l_{s,t}\|$ is small, hence promoting intraregion structure suppression over interregion structure suppression as well as structure localization.

Subsequent work in nonlinear scale-space theory have largely been focused on improving the computation of local conductivities. Catte *et al.* [4] proposed the regularization of $\|\nabla l_{s,t}\|$ using Gaussian regularization priors to improve posedness of the problem. In a similar vein, Yu *et al.* [5] proposed a kernelized approximation of $\|\nabla l_{s,t}\|$ using radial-basis function kernels to improve posedness of the problem as well as structural separability. Black *et al.* [18] take a different approach to improving the posedness of the problem by proposing an alternative conduction coefficient based on robust statistics. Gilboa *et al.* [7] extended the generalized diffusion equation into the complex domain by combining nonlinear diffusion and the free Schrödinger equation and was shown to provide ramp-preserving characteristics. Arridge *et al.* [14] and Undeman and Lindeberg [13] extended the local conduction coefficient using probability theory. It is important to note that these existing probabilistic scale-space formulations differ significantly from the probability scale-space formulation proposed in this study, since the probabilistic aspect of these works stems from the local conduction coefficient, while the probabilistic aspect of the proposed probabilistic scale-space formulation stems from the sampling process. The benefits of the latter approach will be discussed in later sections. Furthermore, the proposed generalized probabilistic scale-space formulation accounts for the observation model, which existing probabilistic scale-space formulations do not.

Another powerful class of nonlinear scale-space formulations with more attractive properties that avoids the "false edge" issues faced by methods based on the model by Perona and Malik [3] are those based on tensor diffusion models [19]. Such methods utilize the local image structure as measured by a second moment matrix to adapt local conductivities and have been shown to allow for good feature detection under noisy scenarios [20].

Given the usefulness of scale-space theory for computer vision applications [16], there is great potential benefit in utilizing scale-space theory for the purpose of image restoration. However, existing scale-space formulations are not designed for the purpose of image restoration and, as such, are limited in this context for several reasons. First, while effective for feature detection, existing scale-space formulations can produce poorly restored images in situations characterized by low signal-to-noise ratios (SNRs) since local information redundancy may be insufficient for image restoration under such situations. Second, existing scale-space formulations also do not account for the observation model and, as such, do not produce accurately restored images when $H$ is not the identity $I$. To apply scale-space theory for the purpose of image restoration, we believe that the definition of scale space should extended to account for the following criteria.

- **Noise robustness**: The presence of noise should have minimal influence on the scale-space realizations at all scales, with the exception of the zeroth scale.
- **Observation model awareness**: The observation model should be taken into consideration.

In Section IIi, we will study scale-space realizations derived using the generalized diffusion equation using probability theory to gain a better understanding of limitations of existing scale-space formulations in the context of image restoration. Furthermore, we will derive the proposed probabilistic scale-space formulation, which addresses the aforementioned criteria.

## III. Sampling-Based Probabilistic Scale-Space Theory

Let $X$ and $Z$ be modeled as Markov random fields (MRFs), where the probability distributions of $X_s$ and $Z_s$ given their local neighborhood $\aleph_s$ is independent of the rest of $x$ and $z$, respectively. Based on probability theory, the scale-space realization $l_{s,t}$ derived from the generalized diffusion equation defined in (5) can be formulated as the expected value of $Z_s$, $\mathrm{E}(Z_s)$, given a conditional probability density function $f(Z_s|\aleph_s)$

$$l_{s,t} = \mathrm{E}(Z_s) = \int_Z Z_s f(Z_s)\,\mathrm{d}Z, \qquad Z \sim f(Z_s|\aleph_s) \tag{7}$$

where $l_{s,0} = z_s$ and $f(Z_s|\aleph_s)$ is estimated in a deterministic manner using all samples from $l_{s,t-1}$ within a local neighborhood around site $s$ weighted by a conduction coefficient $c_{s,t-1}$. Unfortunately, restricting samples to be drawn only from within the local neighborhood around $s$ can result in a poor estimate of $f(Z_s|\aleph_s)$ for image restoration for two reasons. First, since the proximity of samples used to estimate $f(Z_s|\aleph_s)$ to $s$ is very close, there is significant information overlap between the samples. As such, the estimate is biased due to the spatial closeness of the samples to $s$, which can have a negative impact on the quality of the restored image. Second, the number of samples used to estimate $f(Z_s|\aleph_s)$ is small, and, as such, the estimated $f(Z_s|\aleph_s)$ is sensitive to noise, resulting in restored images with low visual quality in situations characterized by low SNRs.

Intuitively, the visual quality of the restored image in situations characterized by low SNRs can be greatly improved by utilizing a more accurate estimate of $f(Z_s|\aleph_s)$. To achieve this goal, we forgo the deterministic estimation approach used in existing scale-space formulations and instead perform a stochastic estimation of the conditional probability distribution $f(Z_s|\aleph_s)$ using a conditional sampling scheme.

Recall that $S$ is a set of sites into a discrete lattice $\mathcal{L}$ and $s \in S$ be a site in $\mathcal{L}$. Let $\Omega$ be a random variable in $S$. To draw a sample $z$ that follows the unknown conditional probability density function $f(Z_s|\aleph_s)$, we first draw a sample $\omega$ from an instrumental distribution $g(\Omega)$. The instrumental distribution $g(\Omega)$ used in the implementation of the proposed formulation is a Gaussian function centered at $s$ with a standard deviation of $\sigma_g = 40$. The motivation behind the use of the aforementioned Gaussian function for the instrumental distribution $g(\Omega)$ is that it promotes samples that are spatially close to $s$ but does not eliminate the possibility of samples that are spatially distant to $s$ (which may still be realizations of $f(Z_s|\aleph_s)$). Let us now introduce the concept of a squared neighborhood gradient magnitude $\|\nabla_{\aleph_s,\aleph_\omega,t}\|_2$, which is defined as the cumulative Gaussian-weighted $\ell^2$-norm between two local neighborhoods

$$\|\nabla_{\aleph_s,\aleph_\omega,t}\|_2 = \sum_{x\in\aleph_s} G_{x-s}\cdot(l_{x,t} - l_{x+\omega-s,t})^2. \tag{8}$$

The associated observation $z(\omega)$ is then either accepted or rejected as a realization of $f(Z_s|\aleph_s)$ based on the following condition:

$$\|\nabla_{\aleph_s,\aleph_\omega,t}\|_2 < \tau \tag{9}$$

where $\tau$ is the rejection threshold. If the condition in (9) holds, then observation $z(\omega)$ is accepted as a realization of $f(Z_s|\aleph_s)$. If the condition does not hold, then $z(\omega)$ is rejected. The conditional sampling process is repeated until an upper bound $\gamma$ for the number of samples to draw from $g(\Omega)$ has been reached. The resulting set of samples

$\{z_{\omega_1}, \ldots, z_{\omega_\gamma}\}$, weighted by a conduction coefficient $c_{s,\omega,t-1}$, provides a significantly more accurate estimate of $f(Z_s|\aleph_s)$ and can then be used to compute the expected value $\mathrm{E}(Z_s)$. In the discrete case, the expected value $\mathrm{E}(Z_s)$ formulated in (7) can be alternatively computed as

$$\mathrm{E}(Z_s) = \frac{\sum_{i=1}^{\gamma} (c_{s,\omega,t})(z_{\omega_i})}{\sum_{i=1}^{\gamma} c_{s,\omega,t}}. \tag{10}$$

The conduction coefficient $c_{s,\omega,t}$ used in the proposed probabilistic scale-space theory extends upon the nonnegative conduction coefficient proposed by Perona and Malik [3] by making $c_{s,\omega,t}$ a function of the squared neighborhood gradient magnitude $\|\nabla_{\aleph_s,\aleph_\omega,t}\|_2$ introduced in (8) and given as

$$c_{s,\omega,t} = \exp\left[-\left(\frac{\|\nabla_{\aleph_s,\aleph_\omega,t}\|_2}{\kappa}\right)\right]. \tag{11}$$

Let $L_t = \{L_{s,t}|s \in S\}$ be an MRF on $S$, where $L_{s,t}$ takes on values representing the scale-space state at site $s$ for scale $t$. Given $\gamma$ samples $\{l_{\omega_1}, \ldots, l_{\omega_\gamma}\}$ drawn from conditional probability density function $f(L_{s,t-1}|\aleph_s)$ using the conditional sampling scheme, the probabilistic scale-space realization $l_{s,t}$ can be computed as

$$l_{s,t} = \mathrm{E}(L_{s,t-1}) = \frac{\sum_{i=1}^{\gamma} (c_{s,\omega,t-1})(l_{\omega_i})}{\sum_{i=1}^{\gamma} c_{s,\omega,t-1}}. \tag{12}$$

It is important to note that the probabilistic scale-space realization $l_{s,t}$ in (12) can be considered a special case of the nonlocal means (NLM) method [23], where, instead of utilizing all samples in the image like in the traditional view of NLM, we are utilizing only a small set of relevant samples drawn from the image. However, this probabilistic sampling process makes a significant difference in terms of both computational efficiency and estimation accuracy. For example, in the case of a $256 \times 256$ image, 65 536 samples used for estimating each pixel based on the traditional view of NLM. However, based on the proposed probabilistic sampling approach, only a small set of samples (e.g., at most 150 samples in our implementation) are needed to estimate each pixel at each scale. Furthermore, the proposed approach achieves improved estimation accuracy due to the use of only relevant samples, which will be illustrated in the experimental results in Section V.

## IV. Generalized Sampling-Based Probabilistic Scale-Space Theory

While the aforementioned computation of $\mathrm{E}(Z_s)$ using the stochastic estimate of $f(Z_s|\aleph_s)$ addresses issues associated with noise, $\mathrm{E}(Z_s)$ is only suitable when the observation model $H$ is the identity $I$. However, many situations are characterized by observation models where $H$ is not the identity $I$, making it important to account for the observation model to construct accurately restored images. Intuitively, given that the underlying goal of image restoration is to recover the original state $x_s$, what we really want to base our generalized probabilistic scale space realization $l_{s,t}$ on is the estimate of $x_s$ given $H$ and $z_s$.

Recall that $x = \{x_s|s \in S\}$ is a realization of random field $X = \{X_s|s \in S\}$. Therefore, given $Z_s \sim (\mathrm{E}[Z_s], \Sigma_{Z_s})$ and $N_s \sim (0, \Sigma_{N_s})$, where $\Sigma_{Z_s}$ and $\Sigma_{N_s}$ are the process and noise covariances, respectively, the estimate of $x_s$ given $H$ and $z_s$ in the Bayesian sense can be expressed as

$$\hat{x}_s = \arg\min_{x_s} \mathrm{E}\left[(\hat{x}_s - x_s)^T(\hat{x}_s - x_s)\right]. \tag{13}$$

Based on the relationship between $x_s$, $z_s$, and $n_s$ established in (1), the Bayesian estimate $\hat{x}_s$ takes the form of

$$\hat{x}_s = \mathrm{A}z_s + b. \tag{14}$$

$A$ and $b$ can be derived based on the unbiasedness and orthogonality conditions of the Bayesian estimator, where the estimator is unbiased and the estimation error is perpendicular to any linear combination of $x_s$ as

$$\mathrm{E}[\hat{x}_s - X_s] = 0 \tag{15}$$

$$\mathrm{E}\left[(\hat{x}_s - X_s)(\alpha Z_s + \beta)^T\right] = 0. \tag{16}$$

Given the unbiasedness condition

$$\begin{aligned} \mathrm{E}[\hat{x}_s - X_s] &= 0 \\ \mathrm{E}[(AZ_s + b) - X_s] &= 0 \\ A\mathrm{E}[Z_s] + b - \mathrm{E}[X_s] &= 0 \\ b &= \mathrm{E}[X_s] - A\mathrm{E}[Z_s]. \end{aligned} \tag{17}$$

Given the orthogonality condition

$$\begin{aligned} \mathrm{E}\left[(\hat{x}_s - X_s)(\alpha Z_s + \beta)^T\right] &= 0 \\ \mathrm{E}\left[(AZ_s + b - X_s)(\alpha Z_s + \beta)^T\right] &= 0 \\ \mathrm{E}\left[(AZ_s + (\mathrm{E}[X_s] - A\mathrm{E}[Z_s]) - X_s)(\alpha Z_s + \beta)^T\right] &= 0 \\ \left(A\mathrm{E}\left[(Z_s - \mathrm{E}[Z_s])Z_s^T\right] - \mathrm{E}\left[(X_s - \mathrm{E}[X_s])Z_s^T\right]\right)\alpha^T &= 0. \end{aligned} \tag{18}$$

For (18) to hold for all values of $\alpha$

$$A\mathrm{E}\left[(Z_s - \mathrm{E}[Z_s])Z_s^T\right] - \mathrm{E}\left[(X_s - \mathrm{E}[X_s])Z_s^T\right] = 0 \tag{19}$$

and so

$$A = \mathrm{E}\left[(X_s - \mathrm{E}[X_s])Z_s^T\right]\mathrm{E}\left[(Z_s - \mathrm{E}[Z_s])Z_s^T\right]^{-1}. \tag{20}$$

Given that

$$\mathrm{E}[HX_s + N_s] = \mathrm{E}[Z_s]$$

$$\mathrm{E}[X_s] = H^{-1}\mathrm{E}[Z_s] \tag{21}$$

$$\mathrm{E}\left[(X_s - \mathrm{E}[X_s])Z_s^T\right] = \Sigma_{Z_s}H^T \tag{22}$$

where $\Sigma_{Z_s}$ is the process covariance, and

$$\mathrm{E}\left[(Z_s - \mathrm{E}[Z_s])Z_s^T\right] = H\Sigma_{Z_s}H^T + \Sigma_{N_s} \tag{23}$$

where $\Sigma_{N_s}$ is the noise covariance, $A$ and $b$ can be rewritten as

$$A = \Sigma_{Z_s}H^T\left(H\Sigma_{Z_s}H^T + \Sigma_{N_s}\right)^{-1} \tag{24}$$

$$b = H^{-1}\mathrm{E}[Z_s] - A\mathrm{E}[Z_s]. \tag{25}$$

Based on $A$ and $b$, the Bayesian estimate of $\hat{x}_s$ based on the expected value $\mathrm{E}(Z_s)$ given $f(Z_s|\aleph_s)$ defined in (7) can be expressed as

$$\hat{x}_s = H^{-1}\mathrm{E}[Z_s] + (H^T {\Sigma_{N_s}}^{-1} H + \Sigma_{Z_s}^{-1})^{-1} \times H^T \Sigma_{N_s}^{-1} (z_s - \mathrm{E}[Z_s]). \quad (26)$$

While (26) provides a nice closed-form solution for $\hat{x}_s$, the covariance matrices $\Sigma_{N_s}$ and $\Sigma_{Z_s}$ and observation model $H$ are not known *a priori* and must be estimated. The approximate solution for $\hat{x}_s$ can be defined as

$$\hat{x}_s = {k_{h_s}}^{-1}\mathrm{E}[Z_s] + \left(\frac{{k_{h_s}}^2}{\hat{\sigma_n^2}} + \frac{1}{\hat{\sigma_{z_s}^2}}\right)^{-1} \frac{k_{h_s}}{\hat{\sigma_n^2}} (z_s - \mathrm{E}[Z_s]) \quad (27)$$

where $k_{h_s}$ is a nonstationary kernel at site $s$, $\hat{\sigma_n^2}$ is the estimated noise variance, and $\hat{\sigma_{z_s}^2}$ is the estimated process variance as defined by

$$\hat{\sigma}_{z_s}^2 = \int_Z (Z_s - \mathrm{E}(Z_s))^2 f(Z_s) \mathrm{d}x. \quad (28)$$

While not the main focus of this study, the nonstationary kernel $k_{h_s}$ can be computed using the method proposed by Joshi *et al.* [22], which allows for the estimation of spatially varying, nonparametric point-spread functions (PSFs) from the observed image. First, a blind sharp image estimation is performed on the observed image, where the edges in the observed image are localized, the corresponding edge profiles are predicted, and an estimated sharp image is computed accordingly. Second, based on this estimated sharp image, a maximum *a posteriori* (MAP) estimation approach is used to estimate the PSF that, when applied to the estimated sharp image, produces the observed image. This approach has been shown to be very effective at estimating nonstationary kernels due to motion, defocus, and intrinsic camera properties [22].

Based on (27), the generalized probabilistic scale-space realization $l_{s,t}$ of $x_s$ can be defined as

$$l_{s,0} = z_s, \quad (29)$$

$$l_{s,t} = {k_{h_{s,t}}}^{-1}\mathrm{E}(L_{s,t-1}) + \left(\frac{{k_{h_{s,t}}}^2}{\hat{\sigma_n^2}} + \frac{1}{\hat{\sigma}_{l_{s,t-1}}^2}\right)^{-1} \times \frac{k_{h_{s,t}}}{\hat{\sigma_n^2}} (z_s - \mathrm{E}(L_{s,t-1})) \quad (30)$$

where, given $\gamma$ samples $\{l_{\omega_1}, \ldots, l_{\omega_\gamma}\}$ drawn from conditional probability density function $f(L_{s,t}|\aleph_s)$ using the conditional sampling scheme, the expected value $\mathrm{E}(L_{s,t})$ is computed as

$$\mathrm{E}(L_{s,t}) = \frac{\sum_{i=1}^{\gamma} (c_{s,\omega,t})(l_{\omega_i})}{\sum_{i=1}^{\gamma} c_{s,\omega,t}} \quad (31)$$

and $\hat{\sigma}_{l_{s,t}}^2$ is computed as

$$\hat{\sigma}_{l_{s,t}}^2 = \frac{1}{\gamma}\sum_{i=1}^{\gamma}(l_{\omega_i} - \mathrm{E}(L_{s,t}))^2. \quad (32)$$

This generalized probabilistic scale-space formulation accounts for both noise and nonidentity observation models, making it well suited for image restoration.

## V. Experiments

The goal of this section is to investigate the effectiveness of the proposed sampling-based generalized probabilistic scale-space formulation at producing accurately restored images. To achieve this goal, we perform a number of experiments involving the restoration of natural images and clinical ultrasound images using the proposed probabilistic scale space formulation. For comparison purposes, three state-of-the-art nonlinear scale-space formulations, as well as the state-of-the-art NLM restoration method [23] were also evaluated. The tested scale-space formulations include the nonlinear diffusion scale space introduced by Perona and Malik [3] (PM), the regularized nonlinear diffusion scale-space proposed by Catte *et al.* [4] (CA), and the complex nonlinear diffusion scale space proposed by Gilboa [7] (GI). All tested formulations were implemented using the parameters proposed in the respective works. The proposed generalized sampling-based probabilistic scale space will be denoted as PS. For testing purposes, the constant $\kappa$ for all tested scale-space formulations was


Fig. 1. Set of test images.

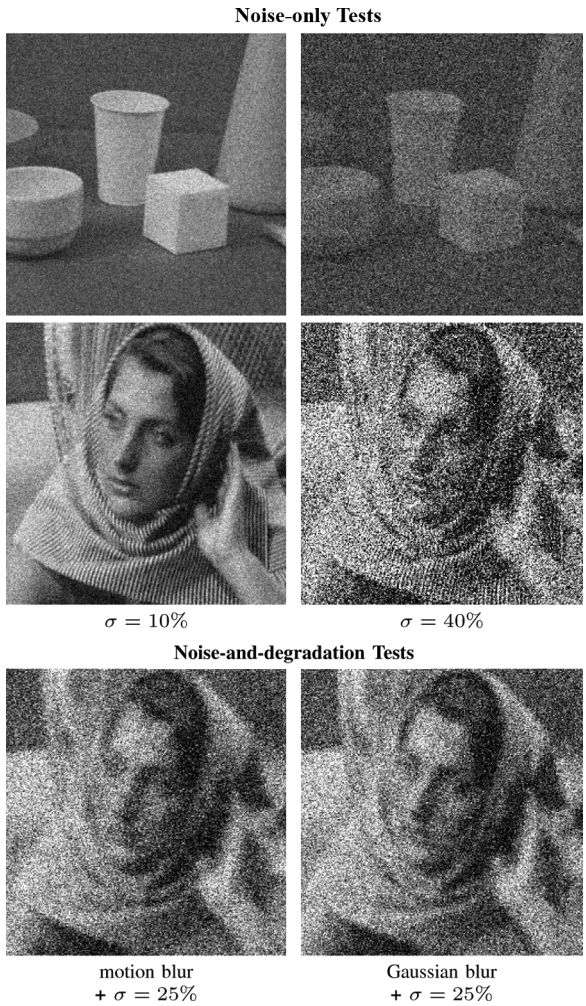


Fig. 2. In the first set of tests, "Scene" and "Barbara" images were corrupted by additive Gaussian noise with a standard deviation of $\sigma = \{10\%, 40\%\}$ of the dynamic range of the image. In the second set of tests, the "Barbara" image was corrupted by motion blur of angle $\theta = 0^\circ$ and length of $d = 5$ and a Gaussian blur with a standard deviation of 3 pixels, as well as additive Gaussian noise with a standard deviation of $\sigma = 25\%$ of the dynamic range of the image.

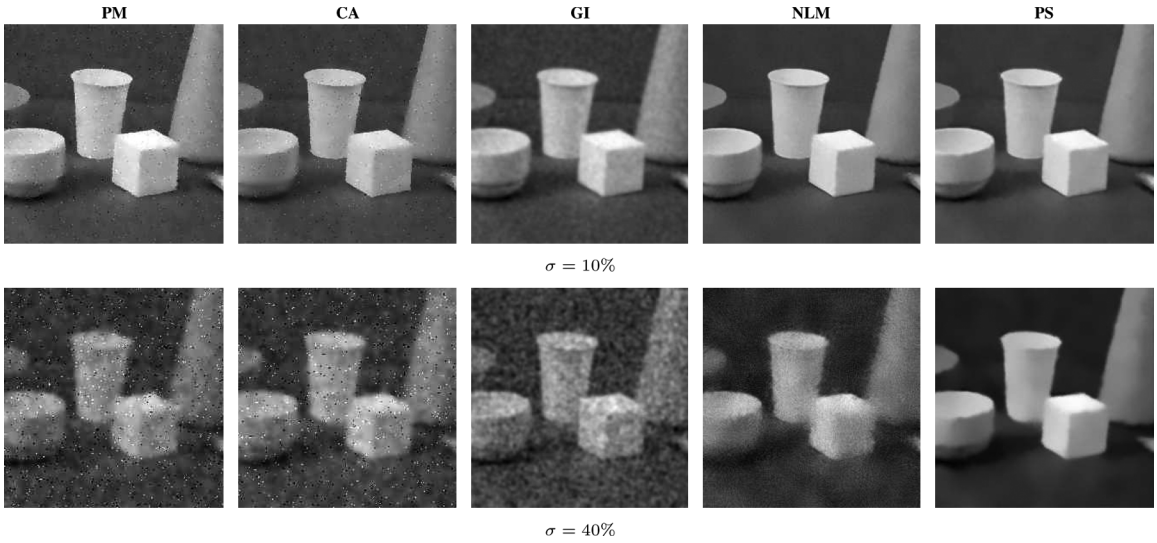


Fig. 3. Restored "Scene" images of the tested scale-space formulations and NLM under additive Gaussian noise with a standard deviation of $\sigma = \{10\%, 40\%\}$ of the dynamic range of the image.

set based on the estimated noise standard deviation $\sigma_n$ of the image. Furthermore, the upper bound $\gamma$ was set to 150 and rejection threshold $\tau = \hat{\sigma}_n^2$, as it was shown to produce stable results during testing for various images. Finally, the local neighborhoods used are $9 \times 9$ rectangular neighborhoods. The set of test images is shown in Fig. 1. Note that both the "Scene" and "Barbara" images used are $256 \times 256$.

### A. Noise and Degradation

To study the effect of noise and image degradation on the restored image produced by the different approaches, two sets of tests were conducted on the test images. For the first set of tests, the "Scene" and "Barbara" test images were corrupted by additive Gaussian noise with standard deviations of $\sigma = \{10\%, 40\%\}$ of the dynamic range of the image. This set of tests is designed to investigate the effect of different noise levels on the restored images. For the second set of tests, the "Barbara" test image was first degraded using two different image degradation models and then corrupted by additive Gaussian noise with a standard deviation of $\sigma = 25\%$ of the dynamic range of the image. The image degradation models used were a motion blur of angle $\theta = 0^\circ$ and length of $d = 5$ and a Gaussian blur with a standard deviation of 3 pixels. This set of tests is designed to investigate the effect of different observation models on the restored images under the presence of noise, with the goal of highlighting the importance of accounting for the observation model during the image restoration process. The degraded and noise corrupted versions of the test images used for testing are shown in Fig. 2. Peak SNR (PSNR) and the mean structural similarity (MSSIM) value [24] was measured to quantify the quality of the restored images.

The PSNR and MSSIM values for the restored images produced using the tested scale-space formulations as well as NLM for the different noise levels are shown in Table I. The proposed probabilistic scale space formulation achieves noticeably higher PSNR and MSSIM when compared with the other tested scale-space formulations and NLM, thus indicating that scale-space theory can be successfully extended for improved image restoration. The restored "Scene" and "Barbara" images produced using the tested scale-space formulations as well as NLM for the different noise levels are shown in Figs. 3 and 4, respectively. For PM and CA, $t = \{20, 30\}$ iterations were used to produce the restored images for $\sigma = \{10\%, 40\%\}$, respectively. For GI, $t = \{10, 15\}$ iterations were used to produce the restored images for $\sigma = \{10\%, 40\%\}$, respectively. For PS, $t = 3$ iterations were used to produce the restored images for both noise cases. The scales are chosen to provide similar levels of noise reduction. Visually, the probabilistic scale space provide noticeably superior structural preservation when compared to the other tested scale-space formulations, hence better satisfying the noise robustness criterion for image restoration. The visual quality of the restored images produced by probabilistic scale space shows improvements to that produced by NLM for both $\sigma = 10\%$ and $\sigma = 40\%$.

TABLE I
PSNR AND MSSIM OF THE RESTORED IMAGES OF THE TESTED SCALE-SPACE FORMULATIONS AND NLM UNDER ADDITIVE GAUSSIAN NOISE WITH A STANDARD DEVIATION OF $\sigma = \{10\%, 40\%\}$ OF THE DYNAMIC RANGE OF THE IMAGE

| **Scene** | | | | |
|---|---|---|---|---|
| **Method** | $\sigma = 10\%$ | | $\sigma = 40\%$ | |
| | **PSNR (dB)** | **MSSIM** | **PSNR (dB)** | **MSSIM** |
| PM | 37.00 | 0.952 | 36.17 | 0.949 |
| CA | 37.00 | 0.952 | 36.26 | 0.949 |
| GI | 36.96 | 0.952 | 36.48 | 0.950 |
| NLM | 45.34 | 0.985 | 37.32 | 0.910 |
| PS | 45.18 | 0.987 | 38.15 | 0.964 |
| **Barbara** | | | | |
| **Method** | $\sigma = 10\%$ | | $\sigma = 40\%$ | |
| | **PSNR (dB)** | **MSSIM** | **PSNR (dB)** | **MSSIM** |
| PM | 24.31 | 0.650 | 20.18 | 0.428 |
| CA | 24.28 | 0.651 | 20.45 | 0.451 |
| GI | 25.18 | 0.720 | 18.67 | 0.313 |
| NLM | 27.75 | 0.811 | 20.90 | 0.457 |
| PS | 29.61 | 0.875 | 22.15 | 0.552 |

The PSNR and MSSIM values for the restored images produced using the tested scale-space formulations as well as NLM for the different image degradation models are shown in Table II. The proposed probabilistic scale-space formulation achieves noticeably higher PSNR and MSSIM when compared to the other tested scale space formulations as well as NLM, thus demonstrating that scale-space theory can be successfully extended for the purpose of image restoration. The restored images produced using the tested scale-space formulations as well as NLM for the different image degradation models are shown in Fig. 5. For PM and CA, $t = 20$ iterations were used to produce the

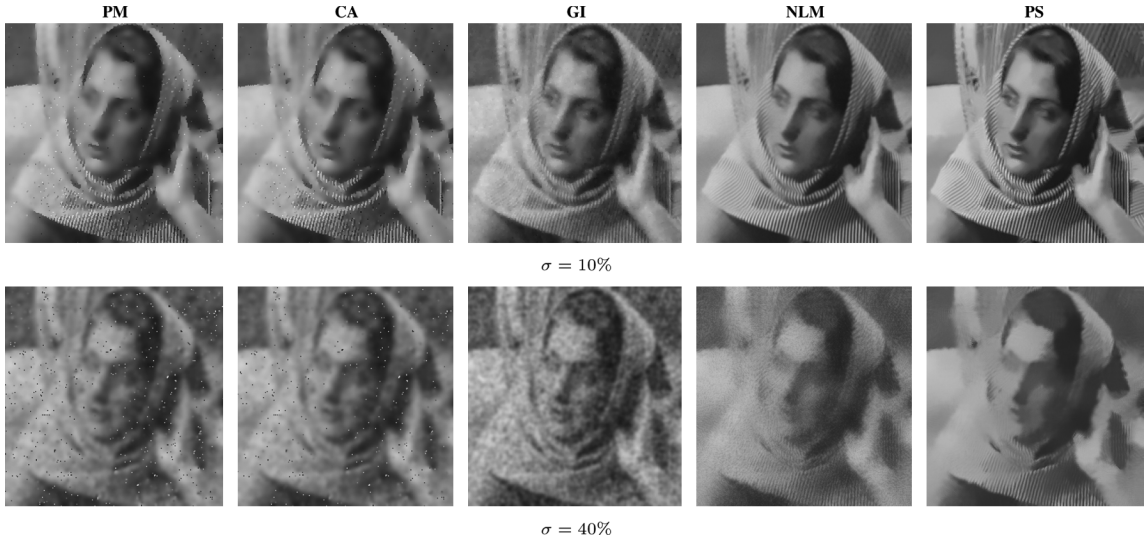


Fig. 4. Restored "Barbara" images of the tested scale-space formulations and NLM under additive Gaussian noise with a standard deviation of $\sigma = \{10\%, 40\%\}$ of the dynamic range of the image.

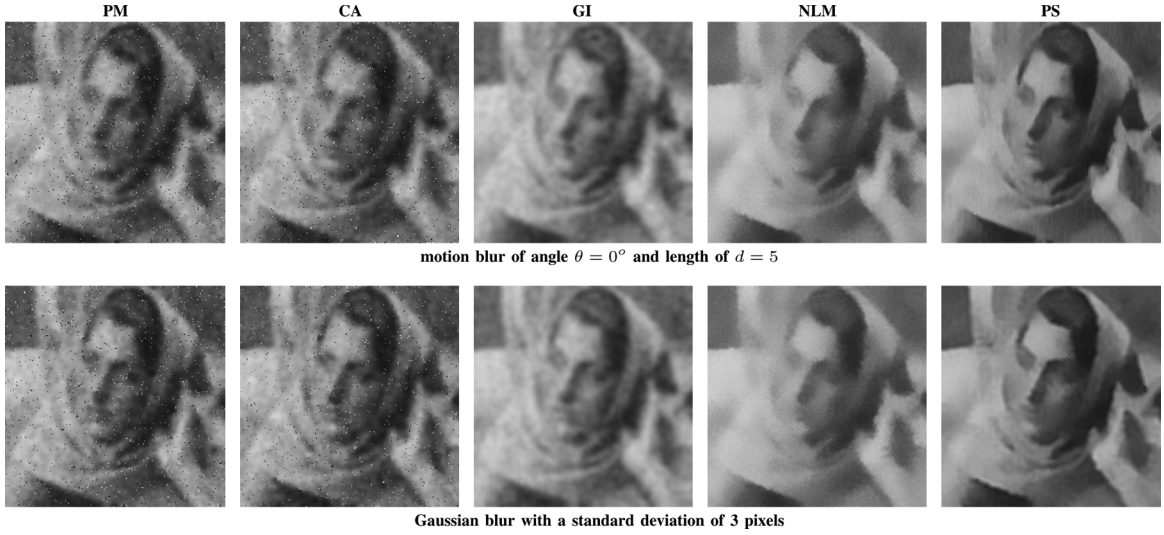


Fig. 5. Restored images of the tested scale-space formulations and NLM under motion blur of angle $\theta = 0^\circ$ and length of $d = 5$ and a Gaussian blur with a standard deviation of 3 pixels, as well as additive Gaussian noise with a standard deviation of $\sigma = 25\%$ of the dynamic range of the image.

TABLE II
PSNR AND MSSIM OF THE RESTORED IMAGES OF THE TESTED SCALE SPACE FORMULATIONS AND NLM UNDER MOTION BLUR OF ANGLE $\theta = 0^\circ$ AND LENGTH OF $d = 5$ AND A GAUSSIAN BLUR WITH A STANDARD DEVIATION OF 3 PIXELS, AS WELL AS ADDITIVE GAUSSIAN NOISE WITH A STANDARD DEVIATION OF $\sigma = 25\%$ OF THE DYNAMIC RANGE OF THE IMAGE

| Method | Gaussian blur | | Motion blur | |
|---|---|---|---|---|
| | PSNR (dB) | MSSIM | PSNR (dB) | MSSIM |
| PM | 18.77 | 0.386 | 18.65 | 0.380 |
| CA | 18.77 | 0.388 | 18.63 | 0.379 |
| GI | 18.77 | 0.385 | 18.63 | 0.379 |
| NLM | 21.07 | 0.425 | 21.30 | 0.440 |
| PS | 22.17 | 0.518 | 22.22 | 0.532 |

restored images for both degradation cases. For GI, $t = 10$ iterations were used to produce the restored image for both degradation cases. For PS, $t = 3$ iterations were used to produce the restored image for both degradation cases. As with the previous set of tests, the restored image produced using probabilistic scale space provide noticeably superior structural restoration when compared with the other tested scale-space formulations as well as NLM, hence better satisfying the observation model criteria. This is due to the fact that the generalized probabilistic scale-space formulation accounts for both noise and the observation model, hence providing more accurately restored images under noise and image degradation.

### *B. Clinical Ultrasound Image*

In the second set of experiments, we study the restored image produced by the generalized sampling-based probabilistic scale-space formulation for a real clinical ultrasound image of the prostate. A total of $t = 3$ iterations were used to produce the restored image. The original image and restored image produced using the proposed probabilistic scale space formulation for the clinical image are shown in Fig. 6. The restored image produced using generalized probabilistic scale space maintains good structural preservation while much of the noise in the original image has been suppressed, hence demonstrating the effectiveness of the generalized probabilistic scale space for producing restored

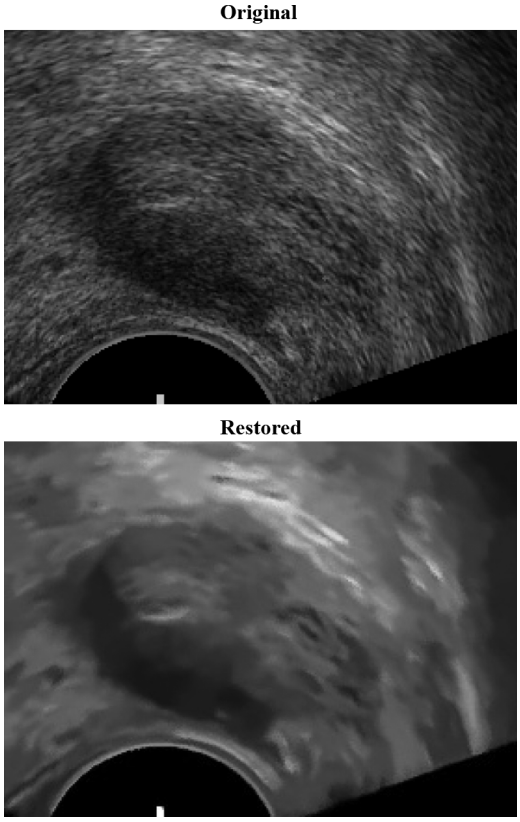


Fig. 6. Original image and restored image produced using the proposed probabilistic scale space formulation for the clinical ultrasound image of the prostate.

images under real-world noise scenarios. The quality of the restored ultrasound image is important for both visualization and midlevel processing such as segmentation, which has potential for improved clinical diagnosis.

## VI. Conclusion and Future Work

In this paper, a novel generalized scale-space framework based on sampling and probabilistic theory for the purpose of image restoration was introduced. The definition of scale space was extended to better account for noise and the observation model, which are important to image restoration. A generalized scale-space formulation was derived based on sampling and probability theory that satisfies the extended scale-space definition for image restoration. The generalized sampling-based scale-space theory was applied to image restoration in 2-D images and experimental results show that improved image restoration performance can be achieved when compared to existing scale-space realizations under situations characterized by low SNRs and image degradation. Future work involves investigating alternative conditional sampling approaches for estimating the conditional probability density functions in a more efficient and effective manner, different conduction coefficients to further improve structural preservation and noise robustness, as well as stopping criteria for determining the optimal number of scales to use.

## References

[1] A. Witkin, "Scale-scale filtering," in *Proc. 7th Int. Joint Conf. Artif. Intell.*, 1983, pp. 1019–1022.

[2] T. Lindberg, "Edge detection and ridge detection with automatic scale selection," in *Proc. IEEE Comput. Soc. Conf. Comput. Vis. Pattern Recogn.*, 1996, pp. 465–470.

[3] P. Perona and J. Malik, "Scale-space and edge detection using anisotropic diffusion," *IEEE Trans. Pattern Anal. Mach. Intell.*, vol. 12, no. 7, pp. 629–639, Jul. 1990.

[4] F. Catte, P. L. Lions, J. M. Morel, and T. Coll, "Image selective smoothing and edge detection by nonlinear diffusion," *SIAM J. Numer. Anal.*, vol. 29, no. 1, pp. 182–193, 1992.

[5] J. Yu, Y. Wang, and Y. Shen, "Noise reduction and edge detection via kernel anisotropic diffusion," *Pattern Recogn. Lett.*, vol. 29, pp. 1496–1503, 2008.

[6] J. Ling and A. Bovik, "Smoothing low-SNR molecular images via anisotropic median-diffusion," *IEEE Trans. Med. Imag.*, vol. 21, no. 4, pp. 377–384, Apr. 2002.

[7] G. Gilboa, N. Sochen, and Y. Zeevi, "Image enhancement and denoising by complex diffusion process," *IEEE Trans. Pattern Anal. Mach. Intell.*, vol. 26, no. 8, pp. 1020–1036, Aug. 2004.

[8] G. Gilboa, "Nonlinear scale space with spatially varying stopping time," *IEEE Trans. Pattern Anal. Mach. Intell.*, vol. 30, no. 12, pp. 2175–2187, Dec. 2008.

[9] J. Maeda, T. Iizawa, T. Ishizaka, C. Ishikawa, and Y. Suzuki, "Segmentation of natural images using anisotropic diffusion and linking of boundary edges," *Pattern Recogn.*, vol. 31, pp. 1993–1996, 1998.

[10] S. Pathak, V. Chalana, D. Haynor, and Y. Kim, "Edge-guided boundary delineation in prostate ultrasound images," *IEEE Trans. Med. Imag.*, vol. 19, no. 12, pp. 1211–1219, Dec. 2000.

[11] R. Manmatha and J. Rothfeder, "A scale space approach for automatically segmenting words from historical handwritten documents," *IEEE Trans. Pattern Anal. Mach. Intell.*, vol. 27, no. 8, pp. 1212–1225, Aug. 2005.

[12] A. Petrovic, O. D. Escoda, and P. Vandergheynst, "Multiresolution segmentation of natural images: From linear to nonlinear scale-space representations," *IEEE Trans. Image Process.*, vol. 13, no. 8, pp. 1104–1114, Aug. 2004.

[13] C. Undeman and T. Lindeberg, "Fully automatic segmentation of MRI brain images using probabilistic anisotropic diffusion and multi-scale watersheds," in *Proc. Scale-Space Conf.*, 2002, vol. 2695, pp. 641–656.

[14] S. Arridge and A. Simmons, "Multi-spectral probabilistic diffusion using Bayesian classification," in *Proc. Scale-Space Conf.*, 1997, vol. 1252, pp. 224–235.

[15] D. Jobson, Z. Rahman, and G. Woodell, "A multiscale retinex for bridging the gap between color images and the human observation of scenes," *IEEE Trans. Image Process.*, vol. 6, no. 7, pp. 965–976, Jul. 1997.

[16] T. Lindeberg, "Scale-space," in *Encyclopedia of Computer Science and Engineering*, B. Wah, Ed. Hoboken, NJ: Wiley, 2009, vol. 4, pp. 2495–2504.

[17] J. Koenderink and A. Van Doorn, "The structure of images," *Biolog. Cybern.*, pp. 363–370, 1984.

[18] M. Black, G. Sapiro, D. Marimont, and D. Heeger, "Robust anisotropic diffusion," *IEEE Trans. Image Process.*, vol. 7, no. 3, pp. 421–432, Mar. 1998.

[19] J. Weickert, *Anisotropic Diffusion in Image Processing*. Stuttgart, Germany: Teubner-Verlag, 1998.

[20] A. Almansa and T. Lindeberg, "Enhancement of fingerprint images using shape-adaptated scale-space operators," *IEEE Trans. Image Process.*, vol. 9, no. 12, pp. 2027–2042, Dec. 2000.

[21] J. von Neumann, "Various techniques used in connection with random digits," *Nat. Bureau Standards Appl. Math Ser.*, vol. 12, pp. 36–38, 1951.

[22] N. Joshi, R. Szeliski, and D. Kriegman, "PSF estimation using sharp edge prediction," in *Proc. IEEE Conf. Comput. Vis. Pattern Recogn.*, 2008, pp. 1–8.

[23] A. Buades, B. Coll, and J. Morel, "Nonlocal image and movie denoising," *Int. J. Comput. Vis.*, vol. 76, no. 2, pp. 123–140, 2008.

[24] Z. Wang, A. Bovik, H. Sheikh, and E. Simoncelli, "Image quality assessment: From error measurement to structural similarity," *IEEE Trans. Image Process.*, vol. 13, no. 4, pp. 600–612, Apr. 2004.